2023

The Weight of New York City: Possible Contributions to Subsidence From Anthropogenic Sources

Tom Parsons

Pei-Chin Wu
University of Rhode Island

Meng (Matt) Wei
University of Rhode Island

Steven D'Hondt
University of Rhode Island, dhondt@uri.edu

Citation/Publisher Attribution

Parsons, T., Wu, P.-C., Wei, M., & D'Hondt, S. (2023). The Weight of New York City: Possible Contributions to Subsidence From Anthropogenic Sources. *Earth's Future, 11*(5), e2022EF003465. https://doi.org/10.1029/2022EF003465
Available at: https://doi.org/10.1029/2022EF003465

The Weight of New York City: Possible Contributions to Subsidence From Anthropogenic Sources

Earth's Future

RESEARCH ARTICLE
10.1029/2022EF003465

The Weight of New York City: Possible Contributions to Subsidence From Anthropogenic Sources

Tom Parsons[1], Pei-Chin Wu[2], Meng (Matt) Wei[2], and Steven D'Hondt[2]

[1]USGS Moffett Field, Moffett Field, CA, USA, [2]Graduate School of Oceanography, University of Rhode Island, Narragansett, RI, USA

Key Points:

- More than 8 million people live in New York City, which is observed to be sinking 1–2 mm/year, while sea level rises
- We calculate the mass of all buildings in New York City and model the subsidence caused by the pressure they exert on the Earth
- We show detailed images of observed subsidence in New York City from satellite data

Supporting Information:

Supporting Information may be found in the online version of this article.

Correspondence to:

T. Parsons,
tparsons@usgs.gov

Citation:

Parsons, T., Wu, P.-C., (Matt) Wei, M., & D'Hondt, S. (2023). The weight of New York City: Possible contributions to subsidence from anthropogenic sources. *Earth's Future*, *11*, e2022EF003465. https://doi.org/10.1029/2022EF003465

Received 6 JAN 2023
Accepted 9 APR 2023

Abstract New York City faces accelerating inundation risk from sea level rise, subsidence, and increasing storm intensity from natural and anthropogenic causes. Here we calculate a previously unquantified contribution to subsidence from the cumulative mass and downward pressure exerted by the built environment of the city. We enforce that load distribution in a multiphysics finite element model to calculate expected subsidence. Complex surface geology requires multiple rheological soil models to be applied; clay rich soils and artificial fill are calculated to have the highest post-construction subsidence as compared with more elastic soils. Minimum and maximum calculated building subsidence ranges from 0 to 600 mm depending on soil/rock physical parameters and foundation modes. We compare modeled subsidence and surface geology to observed subsidence rates from satellite data (Interferometric Synthetic Aperture Radar and Global Positioning System). The comparison is complicated because the urban load has accumulated across a much longer period than measured subsidence rates, and there are multiple causes of subsidence. Geodetic measurements show a mean subsidence rate of 1–2 mm/year across the city that is consistent with regional post-glacial deformation, though we find some areas of significantly greater subsidence rates. Some of this deformation is consistent with internal consolidation of artificial fill and other soft sediment that may be exacerbated by recent building loads, though there are many possible causes. New York is emblematic of growing coastal cities all over the world that are observed to be subsiding (Wu et al., 2022, https://doi.org/10.1029/2022GL098477), meaning there is a shared global challenge of mitigation against a growing inundation hazard.

Plain Language Summary As coastal cities grow globally, the combination of construction densification and sea level rise imply increasing inundation hazard. The point of the paper is to raise awareness that every additional high-rise building constructed at coastal, river, or lakefront settings could contribute to future flood risk, and that mitigation strategies may need to be included. The subsidence mapping concept helps to quantify the hazard and adds specificity to soil types and conditions. We present satellite data that show that the city is sinking 1–2 mm/tr with some areas subsiding much faster.

1. Introduction

Projected sea level rise poses a clear threat to coastal cities, with an expected increase of 200–600 mm by 2050 world-wide (e.g., Griggs et al., 2017). Globally, populations who live in subsiding cities will face rising seas at rates up to four times faster than stable regions (Nicholls et al., 2021). Urban subsidence may be caused by ground water withdrawal, natural ground compaction, tectonic effects, rerouting of normal sediment accumulation, and the weight of cities themselves (Boretti, 2021; Holzer & Galloway, 2005; Li et al., 2021; Parsons, 2021; Piecuch et al., 2018; Russell et al., 2017).

Here we emphasize the major metropolitan area of New York City (population 8.4 million) to look specifically at the cumulative contribution of the built environment on subsidence in detail, something that has not yet been a focus as compared with other factors. New York faces significant challenges from flood hazard; the threat of sea level rise is 3–4 times higher than the global average along the Atlantic coast of North America (Sallenger et al., 2012). Post-glacial isostatic effects are projected to cause between 500–1,500 mm of subsidence by 2100 (Piecuch et al., 2018). Much of lower Manhattan lies between 1 and 2 m in elevation above sea level, and measured subsidence from Global Positioning System (GPS) there is 2.1 mm/year (Boretti, 2021). Greenhouse gas forcing appears to be reducing the natural wind shear barrier along the U.S. east coast, which will allow more frequent high intensity hurricane events in the coming decades (Ting et al., 2019). New York City is ranked third in the world in terms of future exposed assets to coastal flooding (Hanson et al., 2011), and 90% of the 67,400

10.1029/2022EF003465

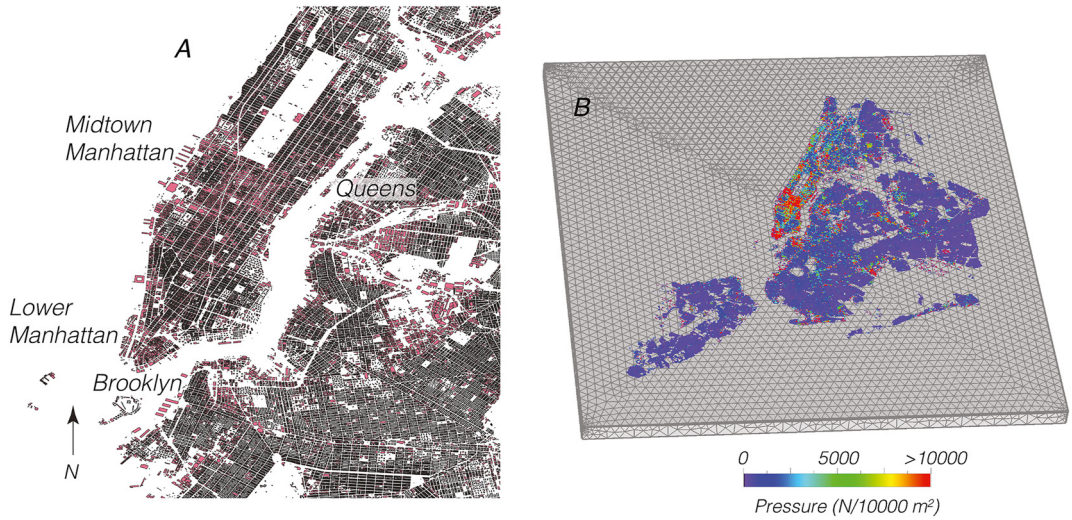

Figure 1. (a) Excerpt from building base outline database for New York City showing parts of Manhattan, Queens, and Brooklyn. Base outlines and height data were used to calculate total building floor areas, which combined with live and dead load values yields a building's mass. (b) The combined building load profile distributed in 100 m-by-100 m cells is shown superposed on the finite element model used to calculate subsidence.

structures in the expanded post-Hurricane-Sandy flood risk areas have not been built to floodplain standards (Dixon et al., 2013).

While broad patterns of natural subsidence are established along the Atlantic margin, this study focuses on a less quantified contribution, localized subsidence caused by buildings. We use the term "subsidence" for any and all downward elevation changes, and we use the engineering term "settlement" for downward elevation changes caused specifically by the weight of buildings. It is well understood that individual buildings settle after construction, and settlement is an accepted factor in most designs (e.g., Wahls, 1962; International Building Code 1808.2, 2021). However, the cumulative settlement effect and broader impact of all buildings has not been studied. There is typically a primary settlement phase that occurs shortly after a building is constructed, and then depending on soil type, there can be an indefinite (Mesri & Vardhanabhuti, 2005) secondary phase of slow creep settlement. Here we calculate the mass of the 1,084,954 buildings within the five boroughs of New York City and model their combined contribution to subsidence for a wide variety of soil conditions.

In this study, the mass of individual buildings is estimated. Local soil conditions can vary significantly, and foundation styles and connection to bedrock also vary. Thus, our calculated settlement values are not as accurate as the individual engineering design values by the builders. However, because building settlement can affect neighboring areas (Alam et al., 2020), we investigate the broader patterns of expected settlement from the combined load of all buildings simultaneously to provide subsidence estimates caused by the built environment. We estimate settlement for surface conditions ranging from bedrock to soft soils to account for uncertainties in localized geology and foundation styles. We compare the spatial patterns of expected subsidence by buildings to detailed elevation changes from satellite interferometry (Interferometric Synthetic Aperture Radar [InSAR]) (Wu et al., 2022), and GPS (Blewitt et al., 2018). We do not expect that the human-built environment explains all observed elevation changes, but rather we highlight its contributions.

2. Building Mass Calculations and Load Distribution

A public database of building base outline and height data was developed by the Microsoft Corporation (https://github.com/Microsoft/USBuildingFootprints/) (Figure 1a). This database was created using a pixel recognition scheme and a conversion to polygons that define building footprints. Testing by Microsoft found that the resulting quality is at least as good as that from hand digitized buildings, with a 93.5% recall rate. We use the open-source Quantum Geographical Information System code to calculate the base area and centroid coordinates of each of the 1,084,954 buildings in New York City. We estimate the number of floors from building heights by assuming

4 m spacing, and the total building area is found by multiplying the base area by the number of floors, assuming that all buildings have straight sides. Knowing the total floor area is useful because the minimum design loads (American Society of Civil Engineers, 2010), give live and dead load criteria as a function of area. The dead load is the weight distribution of the structure itself, and the live load accounts for the contents of the building.

Live load requirements vary for different intended uses, from single family homes (0.48 kN/m^2) to office buildings (2.4 kN/m^2), up to heavy manufacturing facilities (11.97 kN/m^2). We apply an averaged 4.79 kN/m^2 value for live loads. Dead load calculations are based on the construction material densities and vary by structural design. Flooring dead loads range from 0.1 to 3.5 kN/m^2. Reinforced concrete is the most common building material in the world (e.g., Hache et al., 2020), so we use a 2.0 kN/m^2 value for dead loads, which is in the middle range for concrete flooring and walls. From these design criteria the total mass of a building in kg can be calculated by combining live and dead load pressures, dividing by the gravitational constant, and then multiplying by the cumulative building area. The calculated cumulative mass of the buildings in New York City is $7.64 \cdot 10^{11}$ kg (1.68 trillion pounds), which is distributed over a 778.2 km^2 area. The average building mass is $7.04 \cdot 10^5$ kg (1.55 million pounds).

The load profile is calculated by summing individual building mass values into 1,814,701 100 m-by-100 m cells (Figure 1b). This function is converted to surface pressure by multiplying by the gravitational constant, and then dividing by cell area. The loading function is likely an underestimate because it only includes the mass of buildings and their contents, but does not include roads and other paved areas, sidewalks, parks, bridges, railways etc. The load profile is applied to the surface of a finite element model (Figure 1b).

3. Modeling Subsidence From the Urban Load in New York City

Modeling the variable loading function (Figure 1b) from urbanization combined with the complex surficial geology of New York City (Figure 2) requires a finite element approach. The finite element method allows solutions for deformation caused by highly complex applied forces. The problem is broken into a mesh of small pieces (elements) that each deform according to their assigned rheologies and applied loads. The deformation of every element is referred to all the adjoining ones, enabling an overall solution of a system of equations. We use COMSOL Multiphysics® software to build multiple regional soil and bedrock models.

Depth to the bedrock interface is variable under New York City; We use information from 17 boreholes (Nikolaou, 2004) that identify this interface along with mapped surface outcrops (Nikolaou et al., 2001; Tamaro et al., 2000) to interpolate a surface that has a depth range between 0 and 250 m (Figure 2b). The model (Figure 1b) has a soil layer that overlies a hard rock basement layer that extends to 2 km depth. The model is 55 km wide in the east-west direction, and 60 km wide in the north-south orientation. The origin is centered in the model and located at 74°W and 40.7°N. Boundary conditions include a fixed base that cannot move in the vertical direction, and sidewalls that cannot move perpendicular to their orientations. Gravity is enforced. The model is meshed with tetrahedral elements, which are required because of the irregular shape of the basement interface.

The surface geology of New York City is a complex glacial terrane that has several different units that include silt, sand, and clay lake deposits, glacial moraines, outwash and till, beach deposits, and bedrock outcrops. Glacial deposits can have a wide variety of rheological behaviors and are difficult to classify (e.g., Clarke, 2018). In addition, there are significant areas of compressible artificial fill at or near the water line throughout New York City (Figure 2a).

There are more than 1 million buildings involved in the mass calculations that are used to create the load profile, and it is not possible to know the exact foundation circumstances for each one. Generally, building structures that are not connected to bedrock have mat or rafted foundations where a mat is more flexible than a raft; pile foundations have added vertical concrete columns that are emplaced to create enough frictional resistance to counter continued settlement in deep soil layers and may or may not be connected to underlying bedrock (e.g., Poulos, 2016). In New York City most of the largest buildings are located in Manhattan and are directly anchored to bedrock (e.g., Barr et al., 2011). To address this mixture of foundation styles, we calculate a bedrock model (Figure 3) as well as multiple time-dependent linear and nonlinear soil material models from three classes: (a) Modified Cam-Clay models (Roscoe & Burland, 1968), (b) nonlinear elastic models (Hardin & Drnevich, 1972), and (c) linear elastic soil models. For each class, models are run with 25 different parameter sets for Modified Cam-Clay (Devi, 2013; El Kamash & Han, 2014; Heidari et al., 2020; Indraratna & Rujikiatkamjorn, 2004;

10.1029/2022EF003465

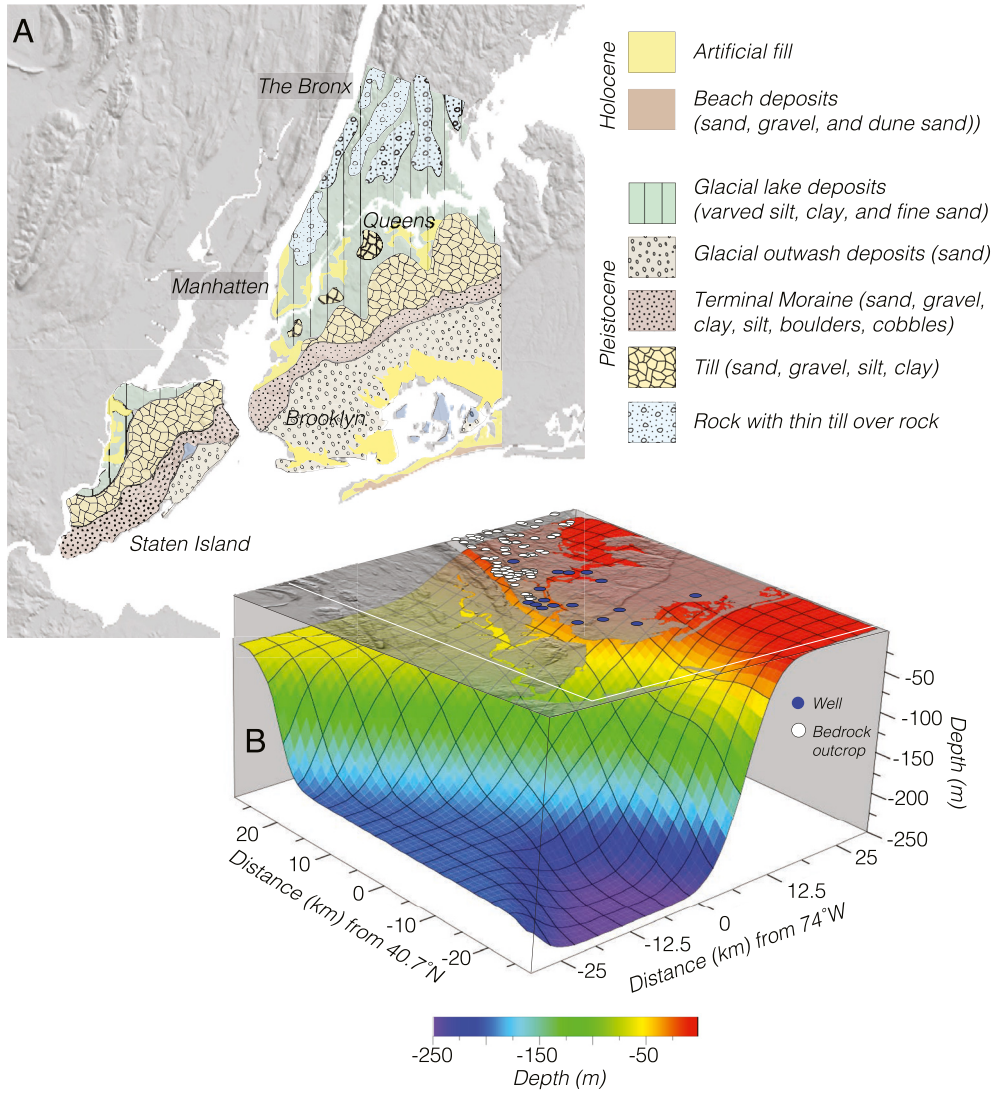

Figure 2. (a) Surface geology map of New York City after Nikolaou et al. (2001) and Tamaro et al. (2000). (b) Soil-bedrock interface interpolated from well data (Nikolaou, 2004) and outcrop observations. Blue dots represent well locations and white dots are bedrock outcrops.

Kodaka et al., 2013; Liu & Carter, 2002; Rujikiatkamjorn & Indraratna, 2006; Sheng et al., 2013; Zhang et al., 2021), the Hardin-Drnevish model (Ahmadp & Ray, 2020; Reid et al., 2004), and elastic soils (Kézdi, 1974; Obrzud & Truty, 2018; Prat et al., 1995) to capture a broad range of soil behaviors.

4. Potential Localized Zones of Subsidence From the Urban Load in New York City

Much as we anticipate sea level rise, hurricanes, and broad tectonic subsidence, we can also examine the contribution of localized patterns of subsidence related to urban concentration. While settlement from individual building projects is expected, calculating the subsidence associated with the combined building load can identify broader patterns where human activity has contributed. We show example maps of calculated subsidence in Figure 3 for three broad soil material models as well as a hard-rock model, where all buildings are assumed to be anchored directly to bedrock without interaction with the soil layer; this result represents minimum subsidence values by elastic compression that range from 0 to 5 mm (Figure 3e).

For building foundations in or on the soil layer, we assume uniform material properties for each general soil model, which is clearly an oversimplification (Figure 2). The glacial geology of New York City can be broken

10.1029/2022EF003465

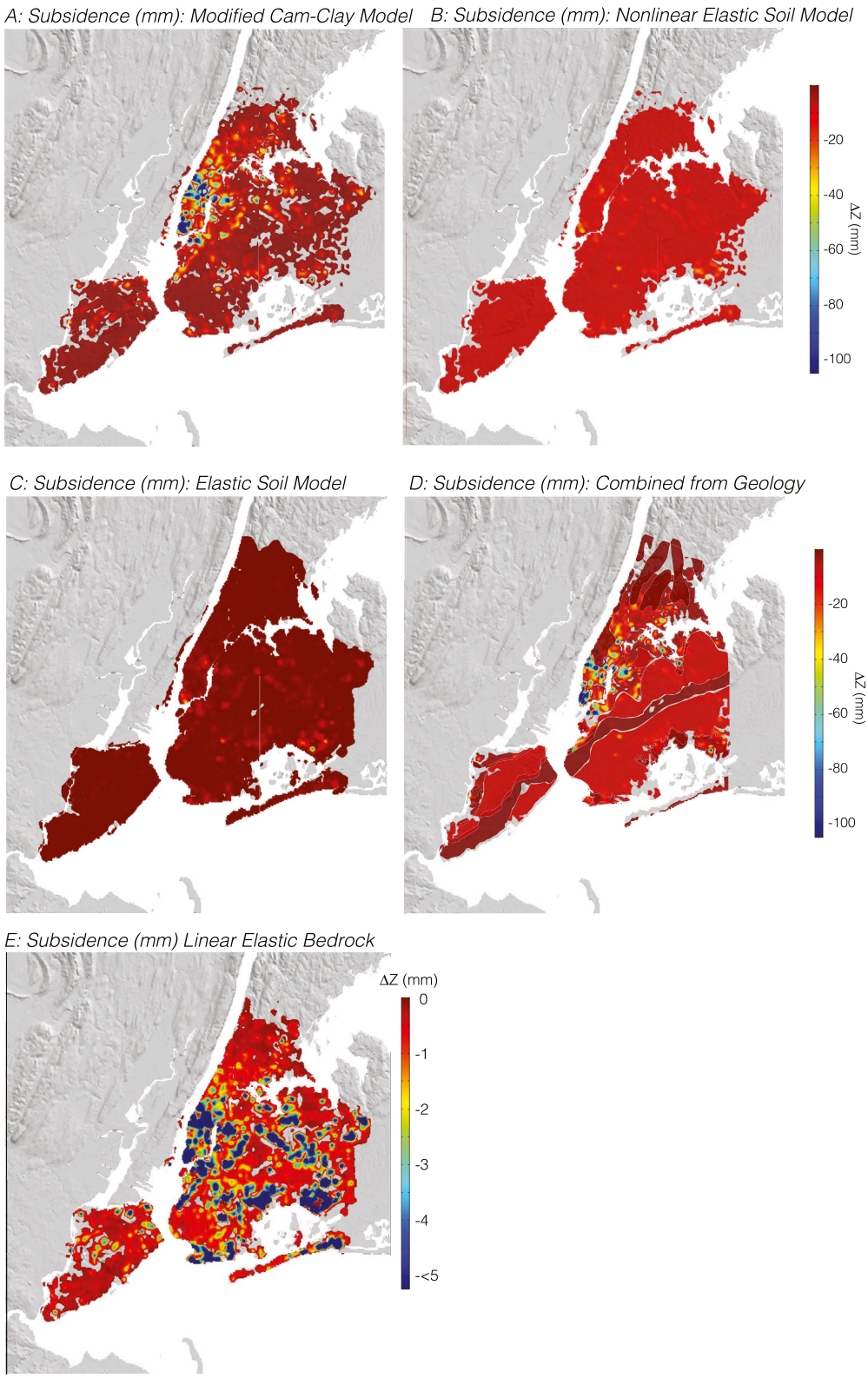

Figure 3.

down into broad units that themselves are comprised of mixed compositions (Nikolaou et al., 2001). The five building subsidence maps shown in Figure 3 have soil layers that range from pure clay soils to hard, unfractured rock. Given the mixed glacial terrane, we assume that the actual subsidence depends on the localized proportions of soil properties. We can begin to partition the response by assigning material properties according to surface geology and associating mapped units with general soil model categories (Figure 3d). In this example we assign artificial fill and clay/silt geology to the Modified Cam-Clay model, the various till units to the nonlinear elastic soil model, the terminal moraine units to the elastic soil model, and the bedrock outcrops to the linear elastic rock model. While this idea begins to differentiate properties spatially, we expect further variation within each of these broad units because each mapped unit is described as a mixture of glaciated materials.

The model layers shown in Figure 3 are predicated on pressure applied at or near the surface from raft, mat, or pile building foundations. However, many if not all, of the largest buildings in Manhattan are anchored directly to bedrock (e.g., Barr et al., 2011) and therefore their expected subsidence is best described by an elastic model (Figure 3f). There are exceptions such as the 57 story Seaport condominium tower at 161 Maiden Lane in Lower Manhattan that relies on a mat and pile foundation (Structure Magazine; https://www.structuremag.org/?p=13197) and may be leaning slightly (e.g., Business Insider, 13 April 2019, https://www.businessinsider.com/photos-nyc-skyscraper-leaning-to-one-side-manhattan-2019-4).

There is a broad range of possible model parameter values that characterize different soil types, which in turn produces associated uncertainty in calculated subsidence (Figure 4). Histograms created from model runs using 25 unique sets of parameters (values are given in Supporting Information S1) from each soil category show wide ranges of primary subsidence values at a given sample point in lower Manhattan (location in Figure 4). The Modified Cam-Clay model subsidence values range from 75 to 600 mm with a median of 294 mm. The nonlinear elastic models show a range between 25 and 425 mm with a median value of 123 mm, and the elastic soil models range between 25 and 375 mm with a median of 61 mm. Bedrock models (Figure 3e) depend only on Young's modulus and do not vary significantly under building loads. Thus the degree of elasticity of soil models governs the maximum settlement under load as can be seen in Figures 4a–4c. While there is considerable uncertainty from input geologic parameters, the spatial patterns of deformation in the maps are consistent in that they all indicate the areas with greatest and least expected subsidence from building loads.

We can compare the range of modeled settlement with observed values from a wide variety of locations and geologic settings from hard rock to sand and silty clay. Du and Gunhan (2014) report from technical documents and job site observations a mean total settlement of 49.7 mm and a range from 2 to 240 mm for 1–7 story buildings in Texas, USA. Katzenbach et al. (2005) observe primary settlement of a 100+ m tower in Frankfurt, Germany at 30 mm, with an expected final value of 50 mm. Mirsayapov and Koroleva (2016) report monitoring data showing 157 mm of settlement in 35 months from a 145 m Russian tower. Hoefsloot and Wiersema (2020) identify secondary settlement rates for buildings greater than 100 m in height with individual values of −0.1 to 0.9 mm/year in Rotterdam, Netherlands, 2.1 mm/year in Montevideo, Uruguay, and 4.4 mm/year in New Orleans, USA. Li et al. (2021) observe surface settlement rates from 145.2 to 24 mm/year in the Beijing Plain with the highest values correlated to highest pressure exerted by building loads. These observed values from individual buildings are smaller than the maximum values from our modeling (up to −600 mm for pure modified cam-clay), which is expected because our modeling is calculated for the effects of multiple buildings in 100 m^2 areas, and for uniform soil models.

The maps in Figure 3 show subsidence values from relatively short term (∼1 year) primary settlement, and do not account for long term secondary settlement that can occur particularly within clay rich layers (e.g., Chen, 2011; Hoefsloot & Wiersema, 2020; Li et al., 2021). Secondary settlement is a result of complex creep and depends strongly on localized soil structures. Modeling it requires detailed knowledge of substrata structure and properties (e.g., Kempfert & Soumaya, 2004). For illustrative purposes (Figure 4d), profiles of one-dimensional secondary

Figure 3. Example subsidence calculations applying the load profile shown in Figure 1b and the soil depth distribution shown in Figure 2b for three soil material models (a) An example modified cam-clay model shows the largest subsidence values (>200 mm) because of the material softness and ability to flow under pressure. (b) Subsidence is shown from a nonlinear elastic model (Hardin & Drnevich, 1972) that is intended to replicate soils of mixed till (which is mostly elastic) with anelastic silt and clay layering, and gives intermediate maximum subsidence values (>100 mm). (c) Subsidence is shown for a purely elastic soil model, which shows the smallest soil values (maximum >50 mm). (d) A combination model corrected for surface geology is shown, and shown in (e) is a model of linear elastic bedrock, which represents the minimum subsidence from building loads, where all foundations are anchored to bedrock and there is no soil compression. Note the different scale from the other models.

10.1029/2022EF003465

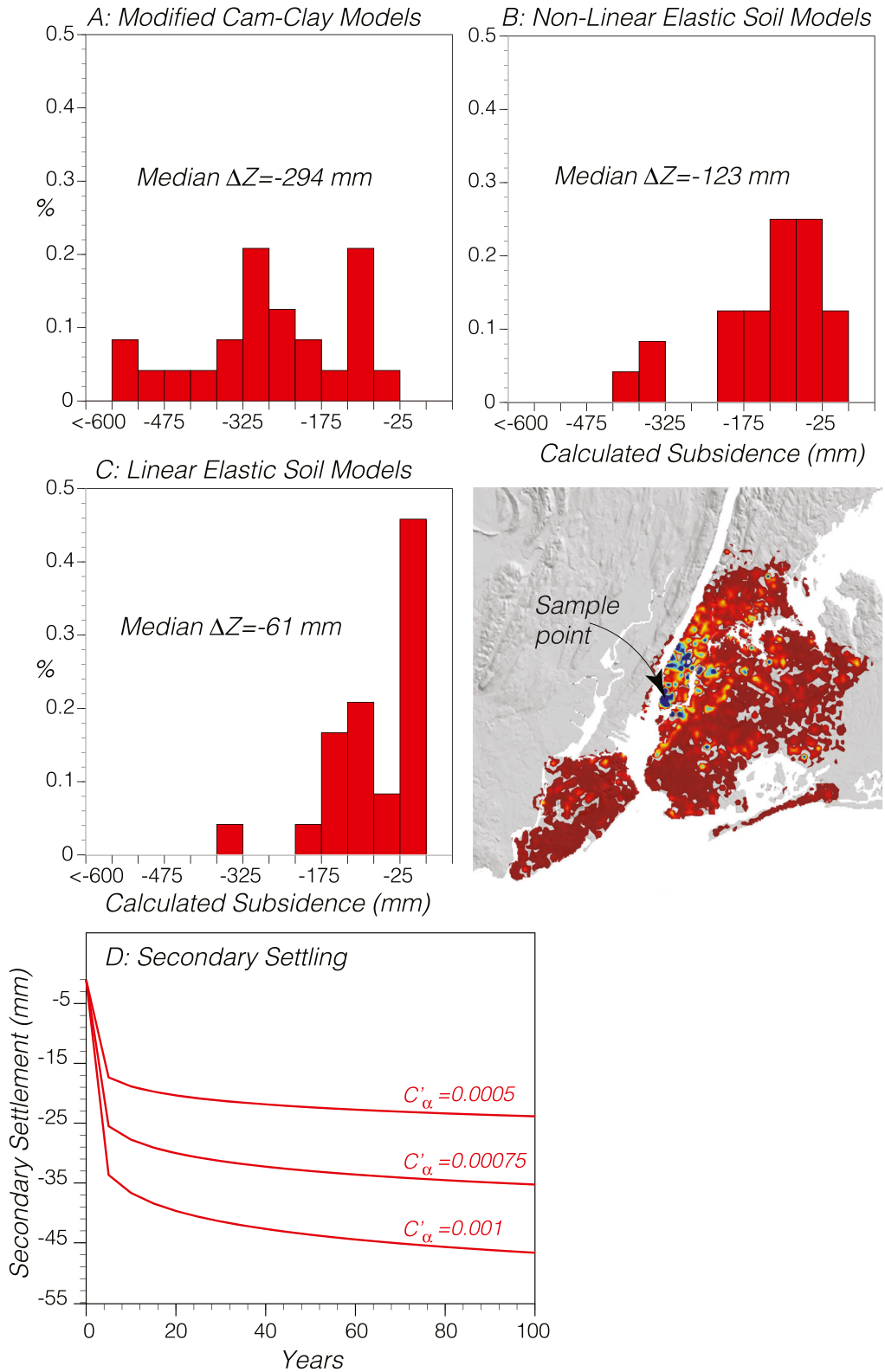

Figure 4. Distributions of 25 each primary subsidence calculations applying a wide range of soil material properties for (a) modified cam-clay models, (b) Hardin-Drnevich nonlinear elastic models, and (c) elastic soil models, with median values given. Values are all taken from the same surface point shown in the map inset. The complex geology of New York City (Figure 2) with its glacially mixed soils requires a broad parameter set to cover the possible range of subsidence responses to loads. (d) A min-mid-max range of secondary settling rate (long-term creep) is shown for clay soils, which can occur after primary settling.

settlement versus time can be calculated using Buisman's (1936) equation that yield characteristic settlement versus time curves as

$$S_c = C'_\alpha H_c \log\left(\frac{t_2}{t_1}\right) \tag{1}$$

where the coefficient of secondary compression C'_α is

$$C'_\alpha = \frac{C_\alpha}{1 + e_p} \tag{2}$$

t_1 and t_2 are start and end times, e_p is the void ratio at the end of primary settlement, and C_α is expressed as

$$C_\alpha = \frac{\Delta e}{\log(t_2/t_1)} \tag{3}$$

where Δe is the change in void ratio. A reasonable range of C'_α values is between 0.0005 and 0.001 (e.g., Mesri, 1973). Example calculations from Parsons (2021) are shown for a 100 years duration in Figure 4d, and give the expected shape that additional, ongoing subsidence could take beneath mat, raft, or pile foundations in clay rich units and/or artificial fill that are present in New York City (Figure 2a). Observations from InSAR show a linear trend of secondary settlement versus time with some seasonal oscillations superposed (Hoefsloot & Wiersema, 2020). These simplified calculations of secondary settlement of ~0.15 mm/year are on the low end of observations that range from 0.1 to 4.4 mm/year. (Hoefsloot & Wiersema, 2020). Subsidence maps related to building settlement capture not only present impacts, but also could convey future problem areas if they consist of poorly consolidated and/or clay rich soils.

5. Observed Subsidence in New York City

Wu et al. (2022) studied subsidence in 99 coastal cities worldwide, including New York City, for the period between 2015 and 2020 using InSAR data. They used six SAR images per year and the Persistent Scatterer method (e.g., Crosetto et al., 2016) to establish the long-term time series of the deformation rate. These observed deformation rates were assumed to be vertical in the absence of strike-slip faulting or active, oil, or gas extraction, none of which apply to New York City. There has been known water pumping and recharge only in the eastern-most part of the city on Long Island (LICAP, 2016). There are 19,326 Persistent Scatterer observation points within the New York City boundaries, which yield a pattern of deformation that is primarily subsidence at a mean rate of -1.77 ± 0.49 (1σ) mm/year (Figure 5a). GPS observations (Blewitt et al., 2018) show a mean vertical change rate of -1.29 ± 0.38 (1σ) mm/year (Figure 5c). The GPS data are consistent with the InSAR mapping, showing subsidence in lower Manhattan, Brooklyn, and Queens as well as on Long Island.

Broad subsidence in New York City is attributed to deglaciation and twentieth Century changes in ice and water loads that have affected much of the Eastern Seaboard of the United States (e.g., Piecuch et al., 2018). Superposed on the postglacial deformation are some localized areas of greater subsidence (Figure 5a). These areas might result from groundwater pumping and/or recharge at rates faster than seasonal recovery, surface erosion and deposition, and other anthropogenic causes such as construction, excavation, and building settlement. We can compare the deformation rate map of New York City with modeled subsidence patterns calculated from the urban building load (Figure 5b) to assess potential contributions from it, recognizing that the building load is only one potential contributor.

InSAR and GPS data map continuous deformation rates (Figure 5), whereas our modeling efforts primarily map effectively instantaneous loading from buildings, many of which were built decades ago. There is more likely a complex time-dependent signature from continuous construction activity that could be a mix of short-term primary settlement and potentially some longer-term superposed secondary settlement depending on soil and foundation types. Observable secondary settlement might result from heavy construction where there are mat, raft, or pile foundations in soft, clay rich soils (e.g., Wahls, 1962; International Building Code 1808.2, 2021). In New York City, buildings that exert the most downward pressure are skyscrapers, but most of these are anchored to bedrock (e.g., Barr et al., 2011). Hard rock elastic compression occurs instantaneously after a load is applied, meaning we do not expect to see ongoing subsidence under some of the largest loads unless the bedrock is heavily

10.1029/2022EF003465

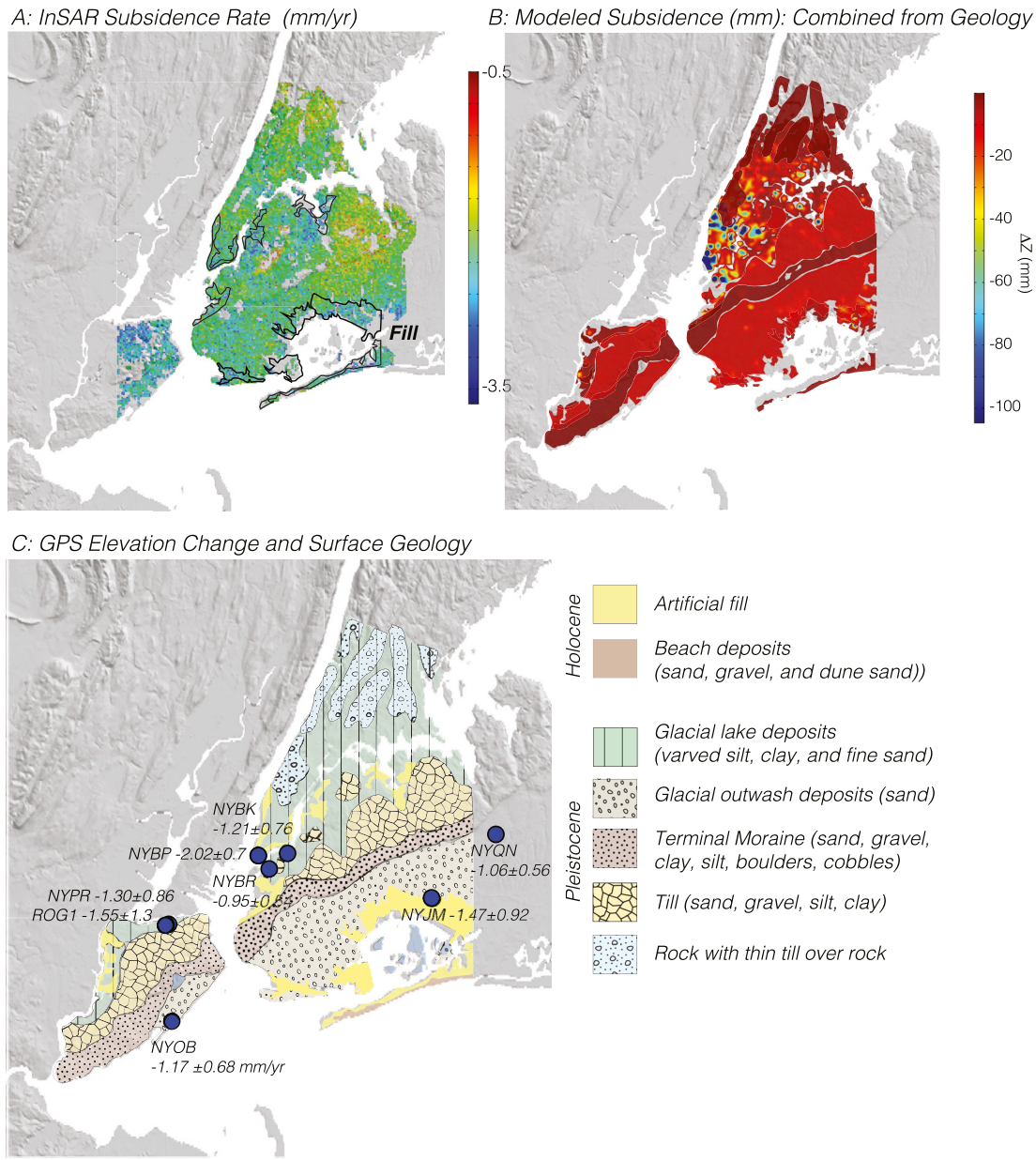

Figure 5. (a) Observed subsidence rates within the New York City boundaries from Interferometric Synthetic Aperture Radar (InSAR) data. The mean rate is -1.77 ± 0.49 (1σ) mm/year. Outlines where artificial fill is mapped (Nikolaou et al., 2001) are shown. Modeled cumulative subsidence from building loads is shown in (b) that is corrected for surface geology for comparison, though we note that multiple processes can influence observed subsidence, such as groundwater pumping and recharge, and post-glacial rebound effects. In (c) Global Positioning System station locations are identified and marked with blue dots along with subsidence rates and uncertainties (Blewitt et al., 2018). Mapped surficial geology is also shown.

fractured. The bedrock geology of Manhattan consists of metamorphosed Schist, Marble, Gneiss and Granodiorite (Merguerian & Baskerville, 1987), and Stumm et al. (2007) characterize it as moderately fractured with a fractured-rock ground-water-flow system that is interconnected. Given these uncertain subsurface conditions, variable timing of construction, and different foundation styles, matching modeled subsidence to current deformation rates is not expected to be directly correlated.

We can highlight the spatial distribution of greatest localized subsidence in New York City that exceeds regional post-glacial deformation by isolating InSAR observations that are subsiding at rates greater than 2 standard deviations from the mean (Figure 6). We see significant subsidence that may be associated with artificial fill (outlined on Figure 6a), as well as in other areas such as Brooklyn, Queens, and northern Staten Island. In Figure 6b, the

10.1029/2022EF003465

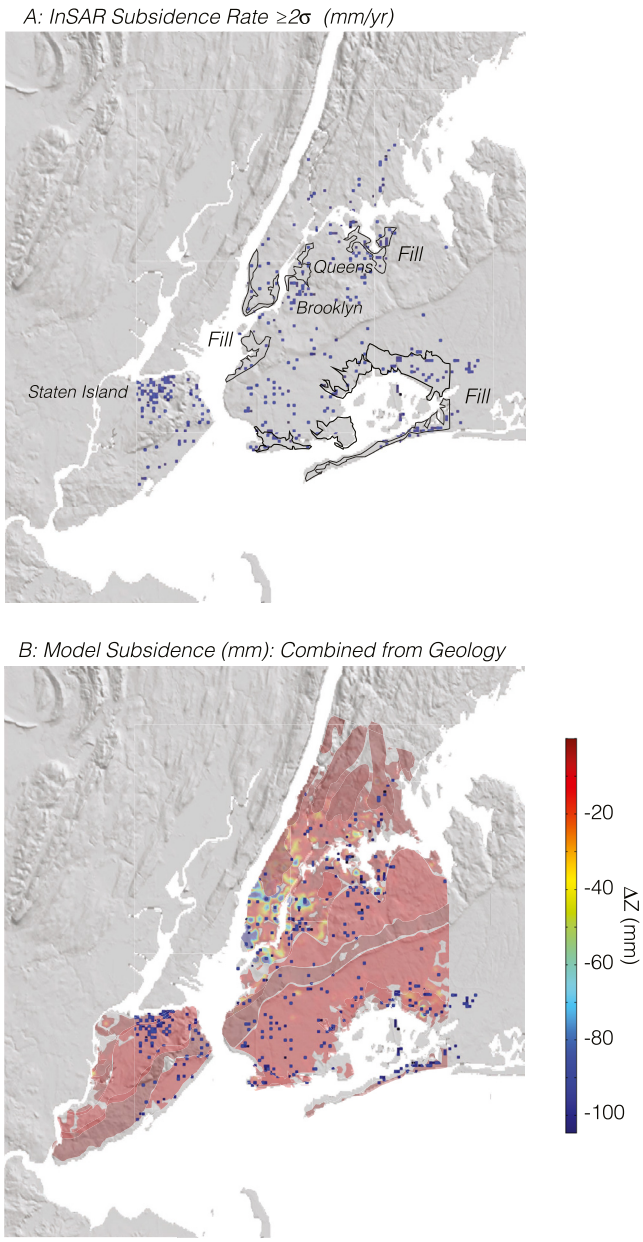

Figure 6. (a) Points are shown with observed subsidence at levels greater than 2 standard deviations below the mean subsidence level of −1.77 mm/year, which is more than −2.75 mm/year. Outlines of mapped areas of artificial fill are shown also. In (b) the same information is shown superposed on modeled subsidence from building loads corrected for surface geology.

significant subsidence pattern is plotted on the modeled subsidence mapping corrected for surface geology from Figure 3d. While there appears to be some correspondence in Lower Manhattan, Brooklyn and Queens, there are other areas of significant subsidence that are clearly not explained by building loads, most notably on northern Staten Island (Figure 6a).

6. Summary and Conclusions

A deeply concentrated population of 8.4 million people faces varying degrees of hazard from inundation in New York City. Two recent hurricanes caused casualties and heavy damage in New York City. In 2012, Hurricane Sandy forced sea water into the city, whereas heavy rainfall from Hurricane Ida in 2021 overwhelmed drainage systems because of heavy runoff within the mostly paved city. The combination of tectonic and anthropogenic subsidence, sea level rise, and increasing hurricane intensity imply an accelerating problem along coastal and riverfront areas. Repeated exposure of building foundations to salt water can corrode reinforcing steel and chemically weaken concrete (e.g., Hobbs, 2001), causing structural weakening.

Additionally, urbanization itself may exacerbate the problem; cumulative pressure applied to the ground from large buildings contributes to subsidence not only from initial primary settlement caused by soil compression and reduction of void space, but also through potential secondary settlement caused by creep in clay rich layers that can continue indefinitely (Mesri & Vardhanabhuti, 2005). Post-construction settlement from individual buildings is expected; in this paper however, we show maps of expected subsidence caused by the cumulative effect of all building loads in New York City. The results depend on near surface geology as well as the underlying bedrock, which influence the severity and longevity of subsidence. Because the surface geology of New York City is a complex glacial terrane, we apply three rheologic soil profiles ranging from a Modified Cam-Clay model to nonlinear soils, linear elastic soil models, and a linear elastic bedrock model. Clay rich soils and artificial fill are especially prone to significant building settlement and clay models show the largest potential subsidence, ranging from −75 to −600 mm with a median of −294 mm at a sample point in lower Manhattan (Figure 4). The nonlinear elastic models show a range between −25 and −425 mm with a median value of −123 mm, and the elastic soil models range between −25 and −375 mm with a median of −61 mm at the same location. Linear elastic bedrock models show subsidence levels that range from 0 to 5 mm. An example deformation map is shown in Figure 3d that assigns different rheological models as appropriate for mapped surface geology. These settlement values are based on the assumption of mat or pile foundations not anchored on bedrock; bedrock foundation settlement is most appropriate to the linear elastic rock model (Figure 3e).

We show maps of observed deformation from InSAR and GPS data that demonstrate an average 1–2 mm/year subsidence rate across New York City (Figure 5), which is consistent with values calculated for post-glacial subsidence across much of the U.S. northeast coast (e.g., Piecuch et al., 2018). There are areas of greater subsidence than predicted from post-glacial effects; we note areas where subsidence is greater than two standard deviations from the mean in Figure 6. Our modeled deformation from building loads is expected to occur shortly after construction, whereas geodetic measurements show ongoing subsidence making comparisons difficult. We do infer some correspondence between significant subsidence and locations of surficial artificial fill that may be consolidating under load. There are also some areas of significant subsidence that correspond with places where secondary building settlement may be occurring, particularly in Brooklyn and Queens (Figure 6a). However, there are many areas of observed strong subsidence where building loads are minor such as on northern Staten Island.

Of particular concern is the possibility of ongoing long-term secondary settlement in densely built areas close to coastlines. Calculated trends shown in Figure 4d show the possibility of very long-term (~100 years) secondary settlement (Mesri & Vardhanabhuti, 2005), and direct observations from InSAR data show 5-year linear settlement trends with no change in slope (Hoefsloot & Wiersema, 2020). It is possible to identify and monitor long-term settlement in urban settings using the Persistent Scatterer method (e.g., Crosetto et al., 2016; Hoefsloot & Wiersema, 2020) with InSAR data.

Additional contributions to subsidence related to urbanization include pumping and/or other discharge of groundwater, and the rerouting of normal sediment accumulation and increased erosion caused by built urban drainage systems (Russell et al., 2017). Damming rivers for water storage further traps sediment supplies and decreases deposition (e.g., Loucks, 2019). Development and filling in of tributaries have cut off nearly all the sediment supply to the East and Harlem Rivers, which in turn has stopped deposition in New York Harbor, increasing the danger of New York City flooding from Nor'easters and hurricanes (Coch et al., 2017).

Major cities around the world are expected to grow disproportionately relative to rural areas, with a projected 70% of the world's population living in cities by 2050 (United Nations, 2019). Major cities on every continent except Antarctica are observed to be subsiding (Wu et al., 2022), and the issue may be worsened as populations grow. Increasing urbanization will likely exacerbate subsidence by groundwater extraction and/or construction density, which combined with accelerating sea level rise implies a growing flood hazard in coastal cities. As these trends continue it will be important to be mindful of accompanying mitigation strategies against inundation in growing coastal cities.

Data Availability Statement

InSAR data used in this research can be downloaded freely online from the Copernicus Open Access Hub from ESA (https://scihub.copernicus.eu/) or the Alaska SAR Facility (https://asf.alaska.edu/). To download, just search Sentinel-1 data for your area of interest and time window. The processing software SNAP (https://step.esa.int/main/download/snap-download/) and StaMPS (https://github.com/dbekaert/StaMPS) are also available online. GPS data were acquired from the Nevada Geodetic Laboratory GPS Networks Map (http://geodesy.unr.edu/NGLStationPages/gpsnetmap/GPSNetMap.html). GPS stations in New York City are operated by the NYC Department of Design and Construction, SmartNet, NOAA National Geodetic Survey, and Topcon Positioning Systems, Inc.

Acknowledgments
We thank Eric Geist and Uri ten Brink (USGS), journal reviewers, and funding from U.S. Geological Survey Coastal and Marine Hazards and Resources Program. Any use of trade, firm, or product names is for descriptive purposes only and does not imply endorsement by the U.S. Government.

References

Ahmadp, M., & Ray, R. (2020). Comparison between Ramberg-Osgood and Hardin-Drnevich soil models in Midas GTS NX. *Pollack Periodica*, *16*(3), 52–57. https://doi.org/10.1556/606.2021.00353

Alam, J., Islam, M. S., Islam, M., & Uddin, N. (2020). Effect of interaction of nearby footings on settlement of foundation under building. *Lecture Notes in Civil Engineering*, *55*, 515–523. https://doi.org/10.1007/978-981-15-0886-8_42

American Society of Civil Engineers. (2010). *Minimum design loads for buildings and other structures* (209 pp.). 3rd Printing (Standard ASCE/SEI 7-10). American Society of Civil Engineers.

Barr, J., Tassier, T., & Trendafilov, R. (2011). Depth to bedrock and the formation of the Manhattan Skyline, 1890–1915. *The Journal of Economic History*, *71*(4), 1060–1077. https://doi.org/10.1017/S0022050711002245

Blewitt, G., Hammond, W. C., & Kreemer, C. (2018). Harnessing the GPS data explosion for interdisciplinary science. *Eos*, *99*. https://doi.org/10.1029/2018EO104623

Boretti, A. (2021). Absolute and relative sea-level rise in the New York City area by measurements from tide gauges and satellite global positioning system. *Journal of Ocean Engineering and Science*, *6*(1), 54–61. https://doi.org/10.1016/j.joes.2020.05.00

Buisman, A. S. K. (1936). Results of long duration settlement tests. In *Proceedings of the 1st international conference on soil mechanics and foundation engineering* (Vol. 1, pp. 103–106).

Chen, X. (2011). *Settlement calculation on high-rise buildings theory and application* (430 pp.). Springer.

Clarke, G. B. (2018). The engineering properties of glacial tills. *Geotechnical Research*, *5*(4), 262–277. https://doi.org/10.1680/jgere.18.00020

Coch, N. K., Lenna, M., & Deely, A. (2017). Anthropogenic land changes and sedimentation response in the tidal straits of New York City. *Journal of Coastal Research*, *33*, 273–285. https://doi.org/10.2112/JCOASTRES-D-16A-00012

Crosetto, M., Monserrat, O., Cuevas-González, M., Devanthéry, N., & Crippa, B. (2016). Persistent scatterer interferometry: A review. *ISPRS Journal of Photogrammetry and Remote Sensing*, *115*, 78–89. https://doi.org/10.1016/j.isprsjprs.2015.10.011

Devi, D. (2013). On the determination of modified cam clay model parameters. *International Journal of Innovative Research in Science, Engineering and Technology*, *3*(Special Issue 4), 250–253.

Dixon, L., Clancy, N., Bender, B., Kofner, A., Manheim, D., & Zakaras, L. (2013). *Flood insurance in New York City following Hurricane Sandy* (131 pp.) Research Report RR-328-NYC. Rand Corporation. https://doi.org/10.7249/RR328

Du, J., & Gunhan, S. (2014). Developing a statistical model for building settlement prediction. In *2014 ASEE annual conference & exposition*. https://doi.org/10.18260/1-2-20280

El Kamash, W., & Han, J. (2014). Displacements of column supported embankments over soft clay after widening considering soil consolidation and column layout: Numerical analysis. *Soils and Foundations*, *54*(6), 1054–1069. https://doi.org/10.1016/j.sandf.2014.11.002

Griggs, G., Árvai, J., Cayan, D., DeConto, R., Fox, J., Fricker, H. A., et al. (2017). *Rising seas in California: An update on sea-level rise science*. California Ocean Science Trust.

Hache, E., Simoën, M., Seck, G. S., Bonnet, C., Jabberi, A., & Carcanague, S. (2020). The impact of future power generation on cement demand: An international and regional assessment based on climate scenarios. *International Economics*, *163*, 114–133. https://doi.org/10.1016/j.inteco.2020.05.002

Hanson, S., Nicholls, R., Ranger, N., Hallegatte, S., Corfee-MorlotHerweijer, J. C., & Chateau, J. (2011). A global ranking of port cities with high exposure to climate extremes. *Climatic Change*, *104*(1), 89–111. https://doi.org/10.1007/s10584-010-9977-4

Hardin, B., & Drnevich, V. (1972). Shear modulus and damping in soils: Design equations and curves. *Journal of the Soil Mechanics and Foundations Division*, *98*(SM7), 667–692. https://doi.org/10.1061/jsfeaq.0001760

Heidari, M., Nikolinakou, M. A., & Flemings, P. B. (2020). Modified Cam-Clay model for large stress ranges and its predictions for geological and drilling processes. *Journal of Geophysical Research: Solid Earth*, *125*(12), e2020JB019500. https://doi.org/10.1029/2020JB019500

Hobbs, D. W. (2001). Concrete deterioration: Causes, diagnosis, and minimising risk. *International Materials Reviews*, *46*(3), 117–144. https://doi.org/10.1179/095066001101528420

Hoefsloot, F., & Wiersema, R. (2020). Evaluation and prediction of high-rise building settlements based on satellite data. In *Tagungsband geomonitoring 2020* (pp. 79–91). https://doi.org/10.15488/9342

Holzer, T. L., & Galloway, D. L. (2005). Impacts of land subsidence caused by withdrawal of underground fluids in the United States. In J. Ehlen, W. C. Haneberg, & R. A. Larson (Eds.), *Humans as geologic agents, reviews in engineering geology* (Vol. 16, pp. 87–99). Geological Society of America. https://doi.org/10.1130/2005.4016(08)

Indraratna, B., & Rujikiatkamjorn, C. (2004). Mathematical modeling and field evaluation of embankment stabilized with vertical drains incorporating vacuum preloading. In *Proceedings, fifth international conference on case histories in geotechnical Engineering, New York, NY, April 13–17, 2004*.

International Building Code. (2021). Retrieved from https://codes.iccsafe.org/content/IBC2021P1

Katzenbach, R., Schmitt, A., & Turek, J. (2005). Assessing settlement of high-rise structures by 3D simulations. *Computer-Aided Civil and Infrastructure Engineering*, *20*(3), 221–229. https://doi.org/10.1111/j.1467-8667.2005.00389.x

Kempfert, H.-G., & Soumaya, B. (2004). Settlement back-analysis of buildings on soft soil in Southern Germany. In *International conference on case histories in geotechnical engineering. 17*. Retrieved from https://scholarsmine.mst.edu/icchge/5icchge/session01/17

Kézdi, A. (1974). *Handbook of soil mechanics* (361 pp.). Elsevier Science.

Kodaka, T., Cui, Y., Mori, S., & Kanematsu, Y. (2013). Soil structure in gravel-mixed sand specimen and its influence on mechanical behavior. In *18th International conference on soil mechanics and geotechnical engineering (Paris)*. Retrieved from https://www.issmge.org/uploads/publications/1/2/369-372.pdf

Li, F., Gong, H., Chen, B., Gao, M., Zhou, C., & Guo, L. (2021). Understanding the influence of building loads on surface settlement: A case study in the central business district of Beijing combining multi-source data. *Remote Sensing*, *13*(16), 3063. https://doi.org/10.3390/rs13163063

LICAP. (2016). State of the aquifer. Retrieved from https://licaponline.com/wpcontent/uploads/2020/08/LICAP_State_of_the_Aquifer_2016.pdf

Liu, M. D., & Carter, J. P. (2002). A structured Cam Clay model. *Canadian Geotechnical Journal*, *39*(6), 1313–1332. https://doi.org/10.1139/T02-069

Loucks, D. P. (2019). Developed river deltas: Are they sustainable? *Environmental Research Letters*, *14*(11), 113004. https://doi.org/10.1088/1748-9326/ab4165

Merguerian, C., & Baskerville, C. A. (1987). The geology of Manhattan Island and the Bronx, New York City, New York. In D. C. Roy (Ed.) *Northeastern Section of the Geological Society of America (Centennial Fieldguide)* (Vol. 5, pp. 137–140).

Mesri, G. (1973). Coefficient of secondary compression. *ASCE Journal of Soil Mechanics and Foundation Division*, *99*(1), 123–137. https://doi.org/10.1061/jsfeaq.0001840

Mesri, G., & Vardhanabhuti, B. (2005). Secondary compression. *Journal of Geotechnical and Geoenvironmental Engineering*, *131*(3), 398–401. https://doi.org/10.1061/(ASCE)1090-0241(2005)131:3(398)

Mirsayapov, I., & Koroleva, I. (2016). Long-term settlements assessment of high-rise building groundbase based on analytical ground deformation diagram. *Procedia Engineering*, *165*, 519–527. https://doi.org/10.1016/j.proeng.2016.11.728

Nicholls, R. J., Lincke, D., Hinkel, J., Brown, S., Vafeidis, A. T., Meyssignac, B., et al. (2021). A global analysis of subsidence, relative sea-level change and coastal flood exposure. *Nature Climate Change*, *11*(4), 338–342. https://doi.org/10.1038/s41558-021-00993-z

Nikolaou, S. (2004). Local geology of New York City and its effect on seismic ground motions. In *International conference on case histories in geotechnical engineering* (Vol. 2). Retrieved from https://scholarsmine.mst.edu/icchge/5icchge/session00g/2

Nikolaou, S., Mylonakis, G., & Edinger, P. (2001). Evaluation of site factors for seismic bridge design in New York City area. *Journal of Bridge Engineering*, *2001*(6), 564–577. https://doi.org/10.1061/(asce)1084-0702(2001)6:6(564)

Obrzud, R., & Truty, A. (2018). *The hardening soil model - A practical guidebook*. Z Soil. PC 100701 report, revised 31.01.2012. Zace Services SA. Retrieved from http://www.zsoil.com

Parsons, T. (2021). The weight of cities: Urbanization effects on Earth's subsurface. *AGU Advances*, *2*(1), e2020AV000277. https://doi.org/10.1029/2020AV000277

Piecuch, C. G., Huybers, P., Hay, C. C., Kemp, A. C., Little, C. M., Mitrovica, J. X., et al. (2018). Origin of spatial variation in US East Coast sea-level trends during 1900–2017. *Nature*, *564*(7736), 400–404. https://doi.org/10.1038/s41586-018-0787-6

Poulos, H. G. (2016). Tall building foundations: Design methods and applications. *Innovative Infrastructure Solutions*, *1*, 10. https://doi.org/10.1007/s41062-016-0010-2

Prat, M., Bisch, E., Millard, A., Mestat, P., & Cabot, G. (1995). *La modelisation des ouvrages* (770 pp.). Hermes.

Reid, J. D., Coon, B. A., Lewis, B. A., Sutherland, S. H., & Murray, Y. D. (2004). *Evaluation of LS-DYNA soil material model 147*. Report No. FHWA-HRT-04-094. Federal Highway Administration.

Roscoe, K. H., & Burland, J. B. (1968). On the generalised stress-strain behaviour of an idealised wet clay. In J. Heyman & F. Leckie (Eds.), *Engineering plasticity* (pp. 535–609). Cambridge University Press.

Rujikiatkamjorn, C., & Indraratna, B. (2006). Three-dimensional analysis of soft soil consolidation improved by prefabricated vertical drains. In *ASCE special geotechnical publication no. 152, Proceedings of Geo-Shanghai 2006, Shanghai, China, 6–8 June 2006* (pp. 161–168).

Russell, K. L., Vietz, G. J., & Fletcher, T. D. (2017). Global sediment yields from urban and urbanizing watersheds. *Earth-Science Reviews*, *168*(2017), 73–80. https://doi.org/10.1016/j.earscirev.2017.04.001

Sallenger, A., Doran, K., & Howd, P. (2012). Hotspot of accelerated sea-level rise on the Atlantic coast of North America. *Nature Climate Change*, *2*(12), 884–888. https://doi.org/10.1038/nclimate1597

Sheng, D., Cui, L., & Ansari, Y. (2013). Interpretation of cone factor in undrained soils via full-penetration finite-element analysis. *International Journal of Geomechanics*, *13*(6), 745–753. https://doi.org/10.1061/(ASCE)GM.1943-5622.0000279

Stumm, F., Chu, A., Joesten, P. K., & Lane, J. W., Jr. (2007). Geohydrologic assessment of fractured crystalline bedrock on the southern part of Manhattan, New York, through the use of advanced borehole geophysical methods. *Journal of Geophysics and Engineering*, *4*(3), 245–252. https://doi.org/10.1088/1742-2132/4/3/S02

Tamaro, G. J., Kaufman, J. L., & Azmi, A. A. (2000). Design and construction constraints imposed by unique geologic conditions in New York. In *Proceedings of the Deep Foundations Institute. 25th Annual meeting and 8th international conference*.

Ting, M., Kossin, J. P., Camargo, S. J., & Li, C. (2019). Past and future hurricane intensity change along the U.S. East Coast. *Scientific Reports*, *9*(1), 7795. https://doi.org/10.1038/s41598019-44252-w

United Nations, Department of Economic and Social Affairs, Population Division. (2019). *World urbanization prospects: The 2018 revision (ST/ESA/SER.A/420)*. United Nations.

Wahls, H. E. (1962). Analysis of primary and secondary consolidation. *ASCE Journal of Soil Mechanics and Foundation Division*, *88*(SM6), 207–234. https://doi.org/10.1061/jsfeaq.0000463

Wu, P.-C., Wei, M. (M.), & D'Hondt, S. (2022). Subsidence in coastal cities throughout the world observed by InSAR. *Geophysical Research Letters*, *49*(7), e2022GL098477. https://doi.org/10.1029/2022GL098477

Zhang, D., Luo, F., Zhu, Z., Liu, J., Li, J., Li, B., & Xue, T. (2021). Study on mechanical properties of gravelly sand under different stress paths. *Advances in Civil Engineering*, *2021*, 1–21. 8898814. https://doi.org/10.1155/2021/8898814